Atmos. Meas. Tech. Discuss., https://doi.org/10.5194/amt-2018-241
Manuscript under review for journal Atmos. Meas. Tech.
Discussion started: 6 August 2018

Atmospheric Measurement Techniques Discussions

A new MesosphEO dataset of temperature profiles from 35 to 85 km using Rayleigh scattering at limb from GOMOS/ENVISAT daytime observations

Alain Hauchecorne[1], Laurent Blanot[2], Robin Wing[1], Philippe Keckhut[1], Sergey Khaykin[1], Jean-Loup Bertaux[1], Mustapha Meftah[1] ,Chantal Claud[3], Viktoria Sofieva[4]

[1]Université Versailles St-Quentin ; Sorbonne Université, CNRS/INSU, LATMOS-IPSL, Guyancourt, France
[2]ACRI-ST, SophiaAntipolis, France
[3]LMD, Ecole Polytechnique, CNRS/INSU, Palaiseau, France
[4]FMI, Helsinki, Finland

Correspondence to: Alain Hauchecorne (alain.hauchecorne@latmos.ipsl.fr)

Abstract. Given that the scattering of sunlight by the Earth's atmosphere above 30-35 km is primarily due to molecular Rayleigh scattering, the intensity of scattered photons can be assumed to be directly proportional to the atmospheric density. From the measured relative density profile it is possible to retrieve an absolute temperature profile by assuming local hydrostatic equilibrium, the perfect gas law, and an a priori temperature from a climatological model at the top of the atmosphere. This technique is applied to Rayleigh lidar observations for over 35 years. The GOMOS star occultation spectrometer included spectral channels to observe daytime limb scattered sunlight close to the star direction. GOMOS Rayleigh scattering profiles in the spectral range 420-480 nm have been used to retrieve temperature profiles in the altitude range 35-85 km with a 2-km vertical resolution. A database of more than 309,000 temperature profiles has been created.

A global climatology was built and compared to GOMOS external model. In the upper stratosphere, where the external model is based on ECMWF analysis, the agreement is better than 2 K. In the mesosphere, where the external model follows MSIS climatology, 5 to 10 K differences are observed. Comparison with nighttime collocated Rayleigh lidar profiles above south of France shows some differences with a vertical structure that may be at least partially explained by the contribution of thermal diurnal tide.

The temperature evolution obtained at Equator indicates the occurrence of mesospheric inversion layers in the temperature profile with global longitudinal extension, descending in about one month from 80 to 70 km. The climatology shows a semi-annual variation in the upper stratosphere, a stratopause altitude varying between 47 and 54 km and an annual variation in the mesosphere.

The technique to derive temperature profiles from Rayleigh scattering at limb can be applied to any other limb-scatter sounder providing observation in the spectral range 350-500 nm. This is also a good candidate for a future small satellite constellation due to the simplicity of the principle.

Atmos. Meas. Tech. Discuss., https://doi.org/10.5194/amt-2018-241
Manuscript under review for journal Atmos. Meas. Tech.
Discussion started: 6 August 2018

1 Introduction

The middle atmosphere (MA: stratosphere and mesosphere, 12 to 90 km altitude) is a transition region between the troposphere, which is heavily influenced by anthropogenic activity, and the upper atmosphere (thermosphere and ionosphere) at the edge of the space and strongly impacted by solar activity. The MA is a unique environment for fundamental research as it is subject to the conjugated influence of climate change, due to anthropogenic activities, and natural solar driven variability.

The increase of GHGs (GreenHouse Gases) induces a global warming at the surface and in the troposphere but also a global cooling in the MA (e.g. Keckhut et al., 2011) induced by the thermal infrared radiation emitted by GHGs escaping directly to the space due to the low optical thickness of the atmosphere above.

The mesosphere is a region where temperature and wind observations are sparse or not well resolved. Recent studies have demonstrated the role of MA dynamics in both tropospheric weather and climate (Baldwin and Dunkerton, 2001; Shaw et al., 2014; Charlton-Perez et al., 2018). Weather and climate-chemisty models are currently moving towards a more comprehensive representation of the MA (Beagley et al., 2000; Baldwin et al., 2003; Hardiman et al., 2010). Atmospheric observations in this region can also be used as a benchmark for climate change studies due to its high sensitivity to the increase of GHGs and to the external solar forcing. Furthermore several applications, such as e.g. the re-entry of space and sub-orbital vehicles, the impact of meteors on the atmosphere and infrasound propagation modelling in the atmosphere, are dependent on the good knowledge of the mesospheric mean state and variability at different scales.

The MA temperature is insufficiently observed above the top altitude of radiosoundings, about 30 km. GNSS (Global Navidation Satellite System) Radio-Occultation technique provides accurate measurements of temperature up to about 35 km with high vertical resolution. Nadir viewing satellite sensors observing in the thermal infrared (SSU: Stratospheric Sounder Unit) and microwave (AMSU: Advanced Microwave Sounding Unit) spectrum provide brightness temperature up to the upper stratosphere (around 45 km) but with very broad vertical weighting functions (≈10 km). These are the only temperature observations assimilated in NWP (Numerical Weather Prediction) models. Limb viewing satellite sounders, e.g. MLS (Microwave Limb Sounder on the Aura satellite) and SABER (Sounding of the Atmosphere using Broadband Emission Radiometry on the TIMED mission), provide temperature profiles up to the upper mesosphere with a good vertical resolution. However these data are not assimilated in NWP models because these instruments are not part of operational meteorological satellite.

The scattering of sunlight (near UV and visible wavelengths) by the Earth atmosphere above the top of the stratospheric layer, about 30-35 km altitude, is only due to Rayleigh scattering by atmospheric molecules. Its intensity is directly proportional to the atmospheric density. It is thus possible to retrieve a temperature profile in absolute value using the hydrostatic equation and the perfect gas law. The temperature is initialized at the top of the profile from a climatological model. This technique has been applied to Rayleigh lidar observations since more than 35 years (Hauchecorne and Chanin, 1980). Rayleigh lidars operated in NDACC (Network for the Detection of Atmospheric Composition Changes) obtain local

observations of the temperature profile between 30 and 80-90 km with a good accuracy and vertical resolution, but in less than 10 locations worldwide. They have been used for trend analysis (Hauchecorne et al., 1991; Keckhut et al., 1995; Li et al., 2011) and or validation of satellite data and identification of possible biases and trends due to orbital changes and instruments ageing (Funatsu et al., 2008; Keckhut et al., 2015; Funatsu et al., 2016).

The observation from space of the Rayleigh scattering at atmospheric limb during daytime may be also used to derive density and temperature profiles in the upper stratosphere mesosphere (US-M). This technique has been applied by Clancy et al. (1994) who derived temperature profiles from 40 to 92 km for the period 1982-1986 using Solar Mesosphere Explorer bright limb observations at 304, 313 and 442 nm. Shepherd et al. (2001) determined temperature profiles from 65 to 90 km during the period March 1992 - January 1994 analysing WINDII/UARS data at 553nm. More recently Sheese et al. (2012) retrieved temperature profiles using OSIRIS/Odin bright limb observations at 318.5 and 347.5 nm in the altitude range 45-85 km. In the frame of the ESA funded MesosphEO project, a new dataset of temperature profiles in the altitude range 35-85 km was created from the analysis of GOMOS/ENVISAT bright limb observations in the spectral band 420-480 nm. A dataset of more than 309,000 profiles from June 2002 to April 2012 is available for climatology and atmospheric dynamics studies.

The paper is organized as follows. In Section 2, the principle of the method is explained and the data processing is described. Section 3 is dedicated to the validation against Rayleigh lidar observations. Section 4 presents the first scientific results with a focus on the evolution of equatorial temperature profiles. Finally, a summary is given in Section 5.

2. Principle and data processing

Method

GOMOS (Global Ozone Monitoring by Occultation of Stars), on board the European Space Agency ENVISAT (ENVIronmental SATellite) platform, was the first operational space instrument dedicated to study the middle atmosphere by the technique of stellar occultations. A description of the instrument as well as an overview of the main scientific results is given in Bertaux et al. (2010). GOMOS observed the spectrum of a star during its occultation by the atmosphere. The atmospheric transmission spectrum is equal to the ratio between the star spectrum absorbed by the atmosphere and the reference star spectrum measured outside the atmosphere. Atmospheric constituents are identified by their absorption spectral features. As the reference spectrum is measured at the beginning of each occultation, we can consider GOMOS as a self-calibrated instrument, independent of any radiometric calibration. Furthermore the stellar occultation technique allows a perfect knowledge of the tangent altitude, depending only on the geometry of the light path between the star and the satellite. The 250-680 nm spectral domain is used for the determination of O_3, NO_2, NO_3 and aerosols from the upper troposphere to the mesosphere (Kyrölä et al., 2010). In addition, two high spectral resolution channels centred at 760 and 940 nm allow measuring respectively O_2 and H_2O. In order to remove the background signal due to the sunlight scattered by the atmosphere, two background spectra are observed just above and below the location of the star, referenced as upper and

lower spectra. In this study we use only these background spectra during daytime (bright limb occultations). Bright limb spectra have been used to derive vertical profiles of ozone during daytime (Tukiainen et al.,). Here we use for each daytime occultation the vertical profile of bright limb light averaged over three 20-nm spectral bands, 420-440 nm, 440-460 nm and 460-480 nm in the upper and lower background spectra. Above about 35 km, the scattering of the sunlight by the stratospheric aerosol layer is negligible and the signal at 420-480 nm is only due to the Rayleigh scattering by atmospheric molecules and, hence, directly proportional to the atmospheric density (at these wavelengths ozone and other trace gases absorption is negligible). Figure 1 shows an example of scattering profile at limb in the 3 spectral bands. The decrease of the Rayleigh scattering signal due to the exponential decrease of the atmospheric density is seen up to about 70 km. Above this altitude the contribution of the measurement noise becomes more important but the Rayleigh signal can be exploited up to at least 90 km after removing this noise.

Data processing

For this study we used the full Level 1 GOMOS database between June 2002 and April 2012 containing 418,000 bright limb occultations. A screening is made to keep only data exploitable to retrieve temperature profiles:

- Occultations with a solar zenith angle larger than 84° are eliminated to avoid spectra with too much absorption between the sun and the limb.
- Profiles, which do not cover the altitude range between 35 and 125 km, are not considered. The lower limit is set to retrieve a temperature profile covering the full altitude range 35-85 km and the upper limit is set to have enough data at the top of the profile to estimate correctly the measurement noise.
- Occultations with the presence of Polar Mesospheric Clouds (PMCs) are also removed. PMCs detection is based on the algorithm described by Pérot et al. (2010). After this screening 309341 occultations are selected.

Processing one occultation

For each spectrum the signal is integrated in the upper and lower background bands of GOMOS spectrometer A2 (400-680 nm) in 3 spectral ranges, 420-440 nm, 440-460 nm and 460-480 nm to obtain 6 profiles versus tangent altitude. After removing the noise contribution straylight and detector noise), estimated at altitudes higher than 110 km and extrapolated at lower altitude, a vertical inversion is performed using an onion peeling method. The resulting 6 profiles of Rayleigh scattering versus altitude are assumed to be proportional to the atmospheric density. The algorithm to retrieve temperature profiles is very similar to Rayleigh lidar algorithm described in details in et al. (2018a). The temperature is computed by downward integration of the hydrostatic equation assuming the perfect gas law:

$$dP = -\rho g(z)dz \qquad (1)$$

Atmos. Meas. Tech. Discuss., https://doi.org/10.5194/amt-2018-241
Manuscript under review for journal Atmos. Meas. Tech.
Discussion started: 6 August 2018

Atmospheric Measurement Techniques Discussions

$$P(z) = \frac{R\rho(z)T(z)}{M} \qquad (2)$$

where z is the altitude, P is the pressure, T the temperature, r the atmospheric density, g the gravity, R the perfect gas constant (R=287.06 J.kg-1K-1) and M the air molar mass (M=28.96). The initialisation of the pressure at the top of the profile is made at about 95 km assuming that the mean temperature in the layer 85-95 km is equal to the temperature of the NRLMSISE-00 climatological model (Picone et al., 2002). For each occultation, 6 individual temperature profiles are retrieved corresponding to 3 selected wavelength intervals and upper and lower panels (Figure 2). For the following, we use only the median profile as a temperature profile corresponding to this occultation, and the dispersion (1 standard deviation) interval of the 6 individual profiles) as an estimation of the its uncertainty.

3. Validation using Rayleigh lidar observations

A validation exercise has been made using the Rayleigh lidar located at Observatoire de Haute Provence (OHP; 43.9°N, 5.7E). This lidar has been part of the Network for Detection of Atmospheric Composition Change (NDACC; http://www.ndsc.ncep.noaa.gov/) since its creation in 1991 and has participated in several satellite validation experiments for instruments on board UARS satellite (Fishbein et al., 1996; Gille et al., 1996; Hervig et al., 1996; Singh et al., 1996; Wu et al. 2003; Keckhut et al., 2004), and more recently for MLS-Aura and SABER-TIMED (Wing et al., 2018b). For the present study GOMOS profiles were selected in a geographical region around OHP (latitude 39°N - 49°N; longitude 9°W – 21°E). Night-mean lidar profiles smoothed down to a 3-km vertical resolution were used for the comparison. A maximum of 12h difference between GOMOS and lidar measurements was accepted for the time coincidence. When several GOMOS profiles reached the coincidence criteria, as shown in Figure 3, the median profile was used for the statistical comparison.

The statistical median difference between OHP lidar and GOMOS temperature (Figure 4) is close to zero below 46 km, negative between 46 and 73 km with down to -5K between 55 and 60 km and again positive above 73 km with up to +7K at 85 km. The dispersion of the differences stays between +/- 5K and +/-7K in the full altitude range. The positive difference in the upper part of the profile may be at least partially due to a warm bias in OHP temperature above 75 km as reported by Wing et al. (2018b) using a comparison with SABER-TIMED. The alternation of positive and negative differences with altitude may indicate a contribution of atmospheric thermal tides, as temperature measurements are not obtained simultaneously. This effect has been already observed when comparisons involved measurements obtained at different solar time (Wild et al., 1995, Keckhut et al., 1996, Keckhut et al. 2015). GOMOS measurements above OHP are performed during daytime at around 11:00 am solar time while lidar operations are conducted during the first part of the night for several hours, with an estimated mid-sequence around 21:00 solar time in average.

To evaluate the potential effect, tidal characteristics above the lidar site have been extracted from the Global Scale Waves Model (GSWM; Hagan et al., 1999). The model has been optimized to provide the migrating thermally forced tides on a global scale throughout the atmosphere on a monthly mean basis. The amplitude and phase of the diurnal and the semi-

diurnal components can be calculated from the outputs of the GSWM-00 tidal model (http://www.hao.ucar.edu/modeling/gswm/gswm. html), which is an extension of the GSWM-98 (Hagan et al., 1999). Such a model has been compared with many observations. While the vertical shape of the observations is well reproduced with this model, the amplitude is often smaller as reported by Jaya Prakash Raju et al. (2010). In this study, the amplitude (Figure 5, left panel) and the phase (Figure 5, middle panel) of the diurnal component of the tides have been extracted from the GSWM for the 45°N latitude for August and middle panels). In the summer period and in the middle atmosphere diurnal component is the dominant one. The expected difference between lidar and GOMOS temperatures is represented in Figure 5, right panel. In the middle mesosphere we observe a +3 K difference while in the vicinity of the mesopause, we note a reverse effect of -3 K. The expected tide contribution does not fully reproduce the observed temperature difference between the OHP lidar and GOMOS but, considering uncertainties associated with the amplitude and phase of the tidal effect, and the fact that non-migrating tides were not taken into account, it appears that at least some part of the observed differences may be explained by local time differences. Further work would be needed to confirm this hypothesis.

4. First scientific results

The monthly climatology of GOMOS temperature has been built by averaging the data into 10° bins from 80°S to 80°N. For each month-latitude bin, the average value is kept only if at least 15 valid profiles are considered. The results are presented in Figure 6. At the stratopause the warmest temperatures are observed at the North Pole from April to September and at the South Pole from November to January, the equatorial stratopause temperature showing relative maximum all around the year. As expected, the coldest temperatures are observed in the upper mesosphere at high latitudes in summer, from May to August in the North hemisphere and from November to February in the South hemisphere. This is due to adiabatic cooling of ascending air in this configuration.

In order to better visualize the main features of the GOMOS climatology, the temperature difference with the GOMOS external model is represented in Figure 7. The GOMOS external model is used for processing of GOMOS data for the retrieval of atmospheric species as described by Kyrölä et al. (2010). For each occultation the external atmospheric profile is built by using ECMWF analysis up to 1 hPa (about 48 km) with a smooth transition to NRLMSISE-00 climatological model above 1 hPa, preserving the hydrostatic equilibrium at all altitudes. Figure 8 shows the average temperature difference between GOMOS and the external model averaged over all latitudes and months. Below 48 km, where the external model is based on ECMWF analysis, the agreement is very good, almost always better than 5 K and in average better than 2 K. The only exception is at 35 km in the equatorial region where GOMOS presents a cold bias compared to the model, especially from January to May (cold bias of about -10 K). We attribute this cold bias to a contamination of the Rayleigh scattering profile by Mie scattering due to the presence of aerosols in the lower stratosphere that may reach 35 km at the equator (Vernier et al., 2009). Above 48 km, where the external model is driven by NRLMSISE-00, the temperature is warmer in

GOMOS data than in the external model up to 80 km by up to +10 K in average at 60 km. Above 80 km GOMOS is colder than the external model.

An interesting characteristic of the geometry of observation is that for a line of sight parallel to the Earth pole axis, the tangent point in the atmosphere is exactly at the Equator. The occultation of Polar Star, with 89.5° declination, gives all around the year a tangent point between 0.8°S and 0.8°N in bright limb conditions. More than 22,000 occultations of the Polar Star have been performed during the 10 years of ENVISAT life, providing a quasi-continuous survey of the temperature evolution at the Equator (Figure 9, left panel). The temperature at the stratopause exhibits a semi-annual variation. In the mesosphere we observe the descent of cold layers from 80 to 70 km in about 1 month. The more intense cold layers occurred in April-May 2007. The vertical profile during the first week of May (Figure 9, right panel) shows that this cold layer corresponds to a so-called mesospheric inversion layer (MIL) in vertical temperature profiles. MILs have been observed by rocketsondes (Schmidlin, 1976) and Rayleigh lidars at middle latitudes (Hauchecorne et al., 1987; Duck et al., 2001), high latitudes (Cutler et al., 2001) and low latitudes (Ratnam et al., 2003). Satellite observations showed the global extend of MILs (Leblanc et al., 1997; Fechine et al., 2008; Gan et al., 2012). Several explanations have been proposed to explain the formation of MILs including gravity wave breaking (Hauchecorne and Maillard, 1990), planetary wave structure (Salby et al., 2002) and thermal tides (Meriwether et al., 1998). Explanations of the long duration and the global longitudinal extend of the observed equatorial MILs are beyond the scope of this paper and will be the topic of a future publication.

Polar Star profiles have been used to build a seasonal climatology at the Equator (Figure 10). In the upper stratosphere the dominant feature is the semi-annual evolution with maxima at equinoxes (February to April and September-October) and minima at solstices (June-July and December). The altitude of the stratopause, taken at the altitude with warmest temperature, varies between 47 and 54 km during the year with a maximum in December-January, a secondary maximum in July. In the mesosphere the evolution is dominated by the annual variation with a maximum in December-January, corresponding to the period with an elevated stratopause, and a long minimum from April to October.

4. Conclusion

A database of more than 309,000 temperature profiles from 35 to 85 km, covering the period June 2002 to April 2012, has been created in the frame of the ESA funded MesosphEO project using the daytime Rayleigh scattering at limb observed by GOMOS.

Comparison with nighttime Rayleigh lidar profiles at OHP shows some differences with a vertical structure that may be at least partially explained by the contribution of thermal diurnal tides.

This data set was used to build temperature climatology as function of latitude and month and to compare it with the GOMOS external model. The agreement is better than 2 K in the upper stratosphere below 48 km (1 hPa) where the model is driven by ECMWF, but 5 to 10 K differences are observed in the mesosphere from 50 to 80 km where the model follows NRLMSISE-00 climatology.

The evolution of the temperature at Equator shows the occurrence of temperature MILs with global longitudinal extension, descending in about one month from 80 to 70 km. The climatology shows a semi-annual variation in the upper stratosphere, a stratopause altitude varying between 47 and 54 km and an annual variation in the mesosphere.

The technique to derive temperature profiles from Rayleigh scattering at limb can be applied to any other limb-scatter sounder providing observation in the spectral range 350-500 nm where the Rayleigh scattering is efficient and the absorption by ozone and other stratospheric constituents not too important. This is also a good candidate for a future small satellite constellation due to the simplicity of the principle.

Acronyms

AMSU: Advanced Microwave Sounding Unit

ECMWF: European Centre for Medium-Range Weather Forecasts

ESA: European Space Agency

ENVISAT: ENVIronmental SATellite

ESA: European Space Agency

GNSS: Global Navidation Satellite System

GOMOS: Global Ozone Monitoring by Occultation of Stars

GSWM: Global Scale Wave Model

MLS: Microwave Limb Sounder on the Aura satellite

NDACC: Network for the Detection of Atmospheric Composition Changes

OHP: Observatoire de Haute Provence

OSIRIS: Optical Spectrograph and InfraRed Imager System

SABER: Sounding of the Atmosphere using Broadband Emission Radiometry

SSU: Stratospheric Sounder Unit

TIMED: Thermosphere Ionosphere Mesosphere Energetics Dynamics

UARS: Upper Atmosphere Research Satellite

WINDII: WIND Imaging Interferometer

Data availability

GOMOS temperature profiles from Rayleigh scattering at limb are freely available at ESA MesosphEO Data product service: http://mesospheo.fmi.fi/data_service.html

Acknowledgments

This work was funded by European Space Agency (MesospEO project), Centre National d'Etudes Spatiales and CNRS/INSU.

References

Baldwin, M. P., and Dunkerton, T. J: Stratospheric harbingers of anomalous weather regime, Science, 294, 581–584, 2001.

Bertaux, J.-L., Kyrölä, E., Fussen, D., Hauchecorne, A., Dalaudier, F., Sofieva, V., Tamminen, J., Vanhellemont, F., Fanton D'Andon, O., Barrot, G., Mangin, A., Blanot, L. , Lebrun, J.-C. , K. Pérot, K. , Fehr, T. Saavedra, , L., Leppelmeier, G. W., and Fraisse, R.: Global ozone monitoring by occultation of stars: an overview of GOMOS measurements on ENVISAT, Atmospheric Chemistry and Physics, European Geosciences Union, 2010, 10 (24), pp.12091-12148, doi 10.5194/acp-10-12091-2010.

Baldwin, M. P., Stephenson, D. B., Thompson, D. W., Dunkerton, T. J., Charlton, A. J., and O'neill, A.: Stratospheric memory and skill of extended-range weather forecasts. Science, 301(5633), 636-640, 2003.

Beagley, S. R., McLandress, C., Fomichev, V. I., and Ward, W. E.: The extended Canadian middle atmosphere model. Geophys. Res. Lett., 27(16), 2529-2532, 2000.

Chapman, S., Lindzen R. S.: Atmospheric Tides. D. Reidel Publishers, Hingham, MA, 1970.

Clancy, R. T., Rusch, D. W., and Callan, M. T.: Temperature minima in average thermal structure of the middle mesosphere (70-80 km) from analysis of 40- to 92-km SME global temperature profiles ; J. Geophys. Res., 99 (D9), 19001-19020, 1994.

Charlton-Perez, A. J., Ferranti, L., and Lee, R. W.: The influence of the stratospheric state on North Atlantic weather regimes. Quarterly Journal of the Royal Meteorological Society (In Press), doi:10.1002/qj.3280, 2018.

Cutler, L. J., Collins, R. L., Mizutani, K., and Itabe, T.: Rayleigh lidar observations of mesospheric inversion layers at Poker Flat, Alaska (65°N, 147°W), Geophys. Res. Lett., 28(8), 1467–1470, doi:10.1029/2000GL012535, 2001.

Duck, T. J., Sipler, D. P., Salah, J. E., and Meriwether, J. W.: Rayleigh lidar observations of a mesospheric inversion layer during night and day, Geophys. Res. Lett., 28(18), 3597–3600, doi:10.1029/2001GL013409, 2001.

Fechine, J., Wrasse, C. M., Takahashi, H., Mlynczak, M. G., and Russell, J. M.: Lower-mesospheric inversion layers over Brazilian equatorial region using TIMED/SABER temperature profiles, Adv. Space Res., 41(9), 1447–1453, doi:10.1016/j.asr.2007.04.070, 2008.

Fishbein E.F., Cofield, R.E., Froidevaux, L., Jarnot, R.F., Lungu, T., Read, W. G., Shippony, Z., Waters, J. W., McDermid, I. S., McGee, T. J., Singh, U., Gross, M., Hauchecorne, A., Keckhut, P., and Gelman, M. E.: Validation of UARS MLS temperature and pressure measurements, J. Geophys. Res., 101, 9983-10016, 1996

Funatsu, B. M., Claud, C., Keckhut, P., and Hauchecorne, A.: Cross-validation of Advanced Microwave Sounding Unit and lidar for long-term upper-stratospheric temperature monitoring, J. Geophys. Res., 113, D23108, doi:10.1029/2008JD010743, 2008.

Funatsu, B., Claud, C., Keckhut, P., Hauchecorne, A., and Leblanc, T.: Regional and seasonal stratospheric temperature trends in the last decade (2002–2014) from AMSU observations. J. Geophys. Res., 121 (14), 8172-8185, doi:10.1002/2015JD024305, 2016.

Gan, Q., Zhang, S. D., and Yi, F.: TIMED/SABER observations of lower mesospheric inversion layers at low and middle latitudes, J. Geophys. Res., 117, D07109, doi:10.1029/2012JD017455, 2012.

Gille, J. C., Bailey, P. L., Massie, S. T., Lyjak, L. V., Edwards, D. P., Roche, A. E., Kumer, J. B. , Mergenthaler, J. L., Hauchecorne, A., Keckhut, P. , McGee, J. T. , McDermid, I. S. , Miller, A. J. , Singh, U., and Swinbank, R.: Accuracy and precision of cryogenic limb array etalon spectrometer (CLAES) temperature retrievals, J. Geophys. Res., 101, 9583-9602, 1996.

Hagan, M. E., Burrage, M. D., Forbes, J. M., Hackney, J., Randel, W. J., and Zhang, X.: GSWM-98: results for migrating solar tides. J. Geophys. Res. 104, 6813–6827, 1999.

Hardiman, S. C., Butchart, N., Osprey, S. M., Gray, L. J., Bushell, A. C., and Hinton, T. J.: The climatology of the middle atmosphere in a vertically extended version of the Met Office's climate model. Part I: Mean state. J. Atmos. Sci., 67(5), 1509-1525, 2010.

Hauchecorne, A., and Chanin, M.-L.: Density and temperature profiles obtained by lidar between 35 and 70 km, Geophys. Res. Lett., 7, 565-568, 1980.

Hauchecorne, A., Chanin, M.-L., and Wilson, R.: Mesospheric temperature inversion and gravity wave breaking, Geophys. Res. Let., 14, 933-936, 1987.

Hauchecorne, A., Chanin, M.-L., and Keckhut, P.: Climatology and trends of the middle atmospheric temperature (33-87 km) as seen by Rayleigh lidar above south of France, J. Geophys. Res., 96, 15297-15309, 1991.

Hauchecorne, A., and Maillard, A.: A 2-D dynamical model of mesospheric temperature inversions in winter, Geophys. Res. Let., 17, 2197-2200, 1990.

Hervig M.E., J.M. Russell III, L.L. Gordley, S. R. Drayson, K. Stone, E. Thompson, M.E. Gelman, I.S. McDermid, P. Keckhut, and Hauchecorne, A.: A validation of temperature measurements from the HAlogen Occultation Experiment, J. Geophys. Res., 101, 10277-10286, 1996.

Jaya Prakash Raju, U., Keckhut, P., Courcoux, Y., Marchand, M., Bekki, S., Morel, B., Bencherif, H., and Hauchecorne, A.: Nocturnal temperature changes over tropics during CAWSES-III campaign: comparison with numerical models and satellite data, Journal of Atmospheric and Solar-Terrestrial Physics, 72, 16, 1171-1179, doi:10.1016/j.jastp.2010.07.013, 2010.

Keckhut P., Hauchecorne, A., and Chanin, M.-L.: Mid-latitude long-term variability of the middle atmosphere: trends, cyclic and episodic changes, J. Geophys. Res., 100, 18887-18897, 1995.

Keckhut P., Gelman, M. E., Wild, J. D., Tissot, F., Miller, A. J. , Hauchecorne, A., Chanin, M.-L., Fishbein, E. F., Gille, J., Russell III, J. M., and Taylor, F.W.: Semi-diurnal and diurnal temperature tides (30-55 km): climatology and effect on UARS-lidar data comparisons, semi-diurnal and diurnal temperature tides (30-55 km): climatology and effect on uars-lidar data comparisons, J. Geophys. Res., special issue on UARS Data Validation, 101, 10.299-10.310, 1996.

Keckhut P., McDermid S., Swart D., McGee T., Godin-Beekmann S., Adriani A., Barnes J., Baray J-L., Bencherif H., Claude H., di Sarra A-G., Fiocco G., Hansen G., Hauchecorne A., Leblanc T., Lee C-H., Pal S., Mégie G., Nakane H., Neuber R., Steinbrecht W., Thayer J.: Review of ozone and temperature lidar validations performed within the framework of the Network for the Detection of Stratospheric Change, J. Environ. Monit., 6 (9), 721-733, 2004.

Keckhut, P., Randel, W.J., Claud, C., Leblanc, T., Steinbrecht, W., Funatsu, B. M., Bencherif, H., McDermid, I.S., Hauchecorne, A., Long, C., Lin, R., and Baumgarten, G.: An evaluation of uncertainties in monitoring middle atmosphere temperatures with the ground-based lidar network in support of space observations, J. Atmos. Sol.-Terr. Phys. doi: 10.1016/j.jastp.2011.01.003, 2011.

Keckhut P., Funatsu, B. M., Claud, C., and Hauchecorne, A.: Tidal effects on stratospheric temperature series derived from successive Advanced Microwave Sounding Unit, Q. J. R. Meteorol. Soc., 141 (687), 477-483. doi: 10.1002/qj.2368, 2015.

Kyrölä E, J. Tamminen, V. Sofieva, J. L. Bertaux, A. Hauchecorne, F. Dalaudier, D. Fussen, F. Vanhellemont, O. Fanton d'Andon, G. Barrot, M. Guirlet, A. Mangin, L. Blanot, T. Fehr, L. Saavedra de Miguel, and R. Fraisse, Retrieval of atmospheric parameters from GOMOS data, Atmos. Chem. Phys., 10, 11881-11903, 2010.

Leblanc, T., and Hauchecorne, A.: Recent observations of mesospheric temperature inversions, J. Geophys. Res., 102(D16), 19,471–19,482, doi:10.1029/97JD01445, 1997.

Li, T., Leblanc, T., McDermid, I. S., Keckhut, P., Hauchecorne, A., and Dou, X.: Middle atmosphere temperature trend and solar cycle revealed by long-term Rayleigh lidar observations, J. Geophys. Res., 116, D00P05, doi:10.1029/2010JD015275, 2011.

Meriwether, J. W., Gao, X., Wickwar, V. B., Wilkerson, T., Beissner, K., Collins, S., and Hagan, M. E.: Observed coupling of the mesosphere inversion layer to the thermal tidal structure, Geophys. Res. Lett., 25, 1479–1482, doi:10.1029/98GL00756, 1998.

Pérot, K., Hauchecorne, A., Montmessin, F., Bertaux, J.-L., Blanot, L., Dalaudier, F., Fussen, D., and Kyrölä, E.: First climatology of polar mesospheric clouds from GOMOS/ENVISAT stellar occultation instrument, Atmos. Chem. Phys., 10, 2723-2735, 2010.

Picone, J. M., Hedin, A. E., Drob, D. P., and Aikin, A. C.: NRLMSISE-00 empirical model of the atmosphere: Statistical comparisons and scientific issues, J. Geophys. Res., Space Physics, 107 (A12), 2156-2202, doi:10.1029/2002JA009430, 2002.

Ratnam, M. V., Nee, J. B., Chen, W. N., Siva Kumar, V., and Rao, P. B.: Recent observations of mesospheric temperature inversions over a tropical station (13.5°N, 79.2°E), *J. Atmos. Sol. Terr. Phys.*, **65**(3), 323–334, doi:10.1016/S1364-6826(02)00337-1, 2003.

Salby, M. L., Sassi, F., Callaghan, P., Wu, D., Keckhut, P., and Hauchecorne, A.: Mesospheric inversions and their relationship to planetary wave structure, J. Geophys. Res., 107(D4), 4041, doi:10.1029/2001JD000756, 2002.

Schmidlin, F. J.: Temperature inversions near 75 km, Geophys. Res. Lett., **3**(3), 173–176, doi:10.1029/GL003i003p00173, 1976.

Shaw, T. A., Perlwitz, J., and Weiner, O.: Troposphere□stratosphere coupling: Links to North Atlantic weather and climate, including their representation in CMIP5 models. Journal of Geophysical Research: Atmospheres, 119(10), 5864-5880, 2014.

Sheese, P. E., Strong, K., Llewellyn, E. J., Gattinger, R. L., Russell III, J. M., Boone, C. D., Hervig, M. E., R. J. Sica, R. J., and Bandoro, J.: Assessment of the quality of OSIRIS mesospheric temperatures using satellite and ground-based measurements, Atmos. Meas. Tech., 5, 2993-3006 , 2012.

Shepherd, M. G., Reid, B., Zhang, S., Solheim, B. H., Shepherd, G. G., Wickwar, V. B., and Herron, J. P.: Retrieval and validation of mesospheric temperatures from Wind Imaging Interferometer observations, J. Geophys. Res., 106 (A11), 24813-24829, 2001.

Singh, U. N., P. Keckhut, A. Hauchecorne, M. Gross, T.J. McGee: Stratospheric temperature measurements by two collocated NDSC lidars at OHP during UARS instrument validation campaign, J. Geophys. Res., 101,10287-10298 , 1996.

Tukiainen, S., E. Kyrölä, P. T. Verronen, D. Fussen, L. Blanot, G. Barrot, A. Hauchecorne, and N. Lloyd, Retrieval of ozone profiles from GOMOS limb scattered measurements, Atmos. Meas. Tech., 4, 659-667, doi:10.5194/amt-4-659-2011, 2011.

Vernier, J. P., Pommereau, J. P., Garnier, A., Pelon, J., Larsen, N., Nielsen, J., Christensen, T., Cairo, F., Thomason, L. W., Leblanc, T., and McDermid, I. S.: The tropical stratospheric aerosol layer from CALIPSO lidar observations, J. Geophys. Res., 114, D00H10, doi:10.1029/2009JD011946, 2009.

Wild, J. D., Gelman, M. E., Miller, A. J., Chanin, M.-L., Hauchecorne, A., Keckhut, P., Farley, R., Dao, P. D., Gobbi, G. P., Adriani, A., Congeduti, F., McDermid, I. S., McGee, T. J., and Fishbein, E.F.: Comparison of stratospheric temperature from several lidars using NMC and MLS data as transfer reference, J. Geophys. Res., 100, 11.105-11.111, 1995.

Wing, R., Hauchecorne, A., Keckhut, P., Godin-Beekmann, S., Khaykin, S., McCullough, E., Mariscal, J.-F., and D'Almeida, E.: Lidar temperature series in the middle atmosphere as a reference data set. Part A: Improved retrievals and a 20 year cross-validation of two co-located French lidars, Atmos. Meas. Tech., (Under Review), doi 10.5194/amt-2018-13, 2018a.

Wing, R., Hauchecorne, A., Keckhut, P., Godin-Beeckmann, S., Khaykin, S., and McCullough, E.: Lidar temperature series in the middle atmosphere as a reference data set. Part B: Assessment of temperature observations from MLS/Aura and SABER/TIMED satellites Atmospheric Measurement Techniques, (Under Review), doi 10.5194/amt-2018-13, 2018b.

Wu, D. L., Read, W. G., Shippony, Z., Leblanc, T., Duck, T.J., Ortland, D.A., Sica, R.J., Argall, P.S., Oberheide, J., Hauchecorne, A., Keckhut, P., She, C. Y., and Krueger, D. A.: Mesospheric temperature from UARS MLS: retrieval and validation, J. Atmos. Sol. Terr. Phys., 65, 245-267, 2003.

Atmos. Meas. Tech. Discuss., https://doi.org/10.5194/amt-2018-241
Manuscript under review for journal Atmos. Meas. Tech.
Discussion started: 6 August 2018

Atmospheric Measurement Techniques Discussions

Figures

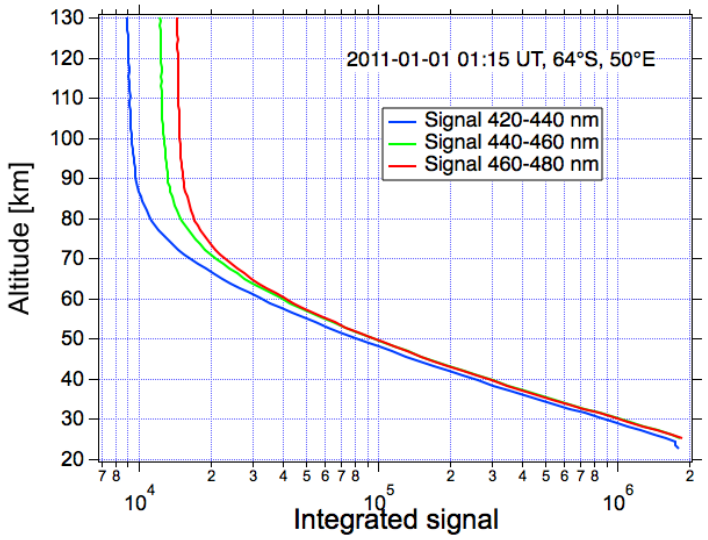

Figure 1: Spectrometer signal integrated in the three 20-nm spectral ranges for one occultation on 1st January 2011 (star ID =3, orbit number = 46209), lower background spectrum.

5

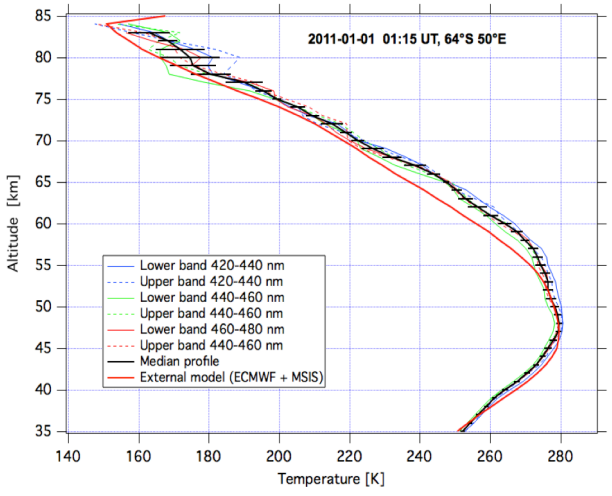

Figure 2. Temperature profiles processed for the same occultation as in Figure 1. The horizontal bar indicates the dispersion (1 standard deviation) between the 6 individual profiles.

Atmos. Meas. Tech. Discuss., https://doi.org/10.5194/amt-2018-241
Manuscript under review for journal Atmos. Meas. Tech.
Discussion started: 6 August 2018

Atmospheric Measurement Techniques Discussions

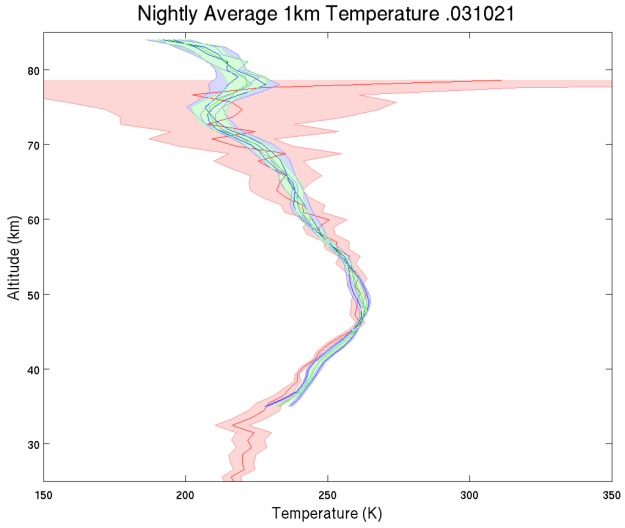

Figure 3: Example of comparison between a Rayleigh lidar profile at OHP on 21st October 2003 (in red) and two collocated GOMOS profiles selected using the co-location criteria (in blue and green). When two or more GOMOS profiles are selected, the median profile is used for the statistical comparison. For the lidar profile (red), each individual GOMOS profile (blue) and the median GOMOS profile (green), the standard deviation of its uncertainty is represented by the shaded area.

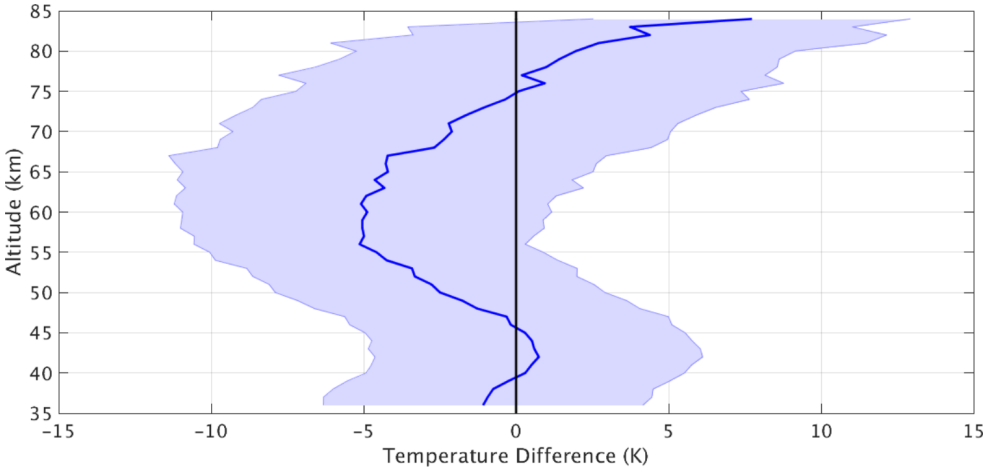

Figure 4. Statistical median temperature difference between OHP lidar and GOMOS temperature profiles (lidar minus GOMOS temperature). The shaded area represents the dispersion of the differences (one standard deviation).

Atmos. Meas. Tech. Discuss., https://doi.org/10.5194/amt-2018-241
Manuscript under review for journal Atmos. Meas. Tech.
Discussion started: 6 August 2018

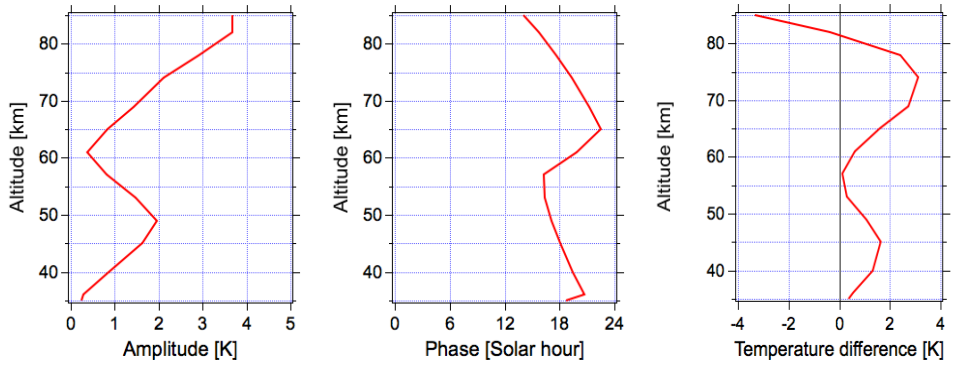

Figure 5. Amplitude (leftpanel) and phase (time of the maximum temperature; righpanel) of the diurnal tides extracted from the GSWM above 45°N for August. Temperature differences (lidar minus GOMOS; right panel) expected from diurnal atmospheric tides as simulated by the GSWM-00 model.

Atmos. Meas. Tech. Discuss., https://doi.org/10.5194/amt-2018-241
Manuscript under review for journal Atmos. Meas. Tech.
Discussion started: 6 August 2018

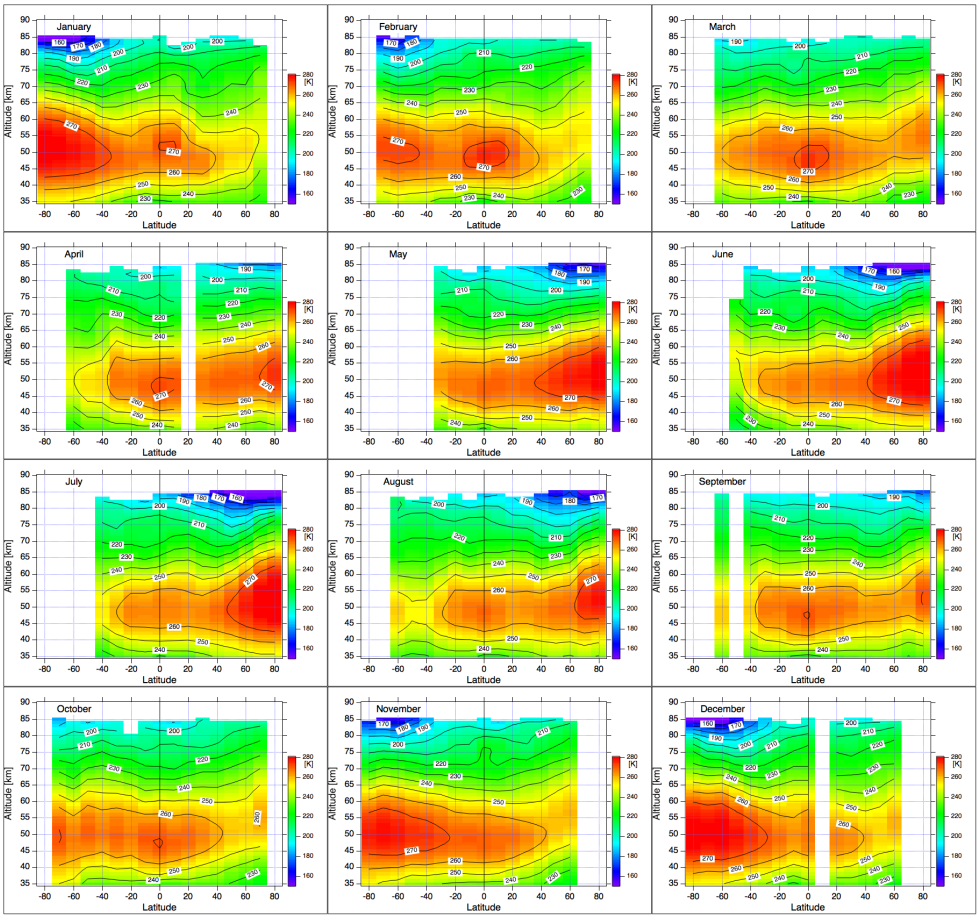

Figure 6. Monthly climatology of GOMOS Rayleigh temperature. Data are averaged over 10° latitude bins.

Atmos. Meas. Tech. Discuss., https://doi.org/10.5194/amt-2018-241
Manuscript under review for journal Atmos. Meas. Tech.
Discussion started: 6 August 2018

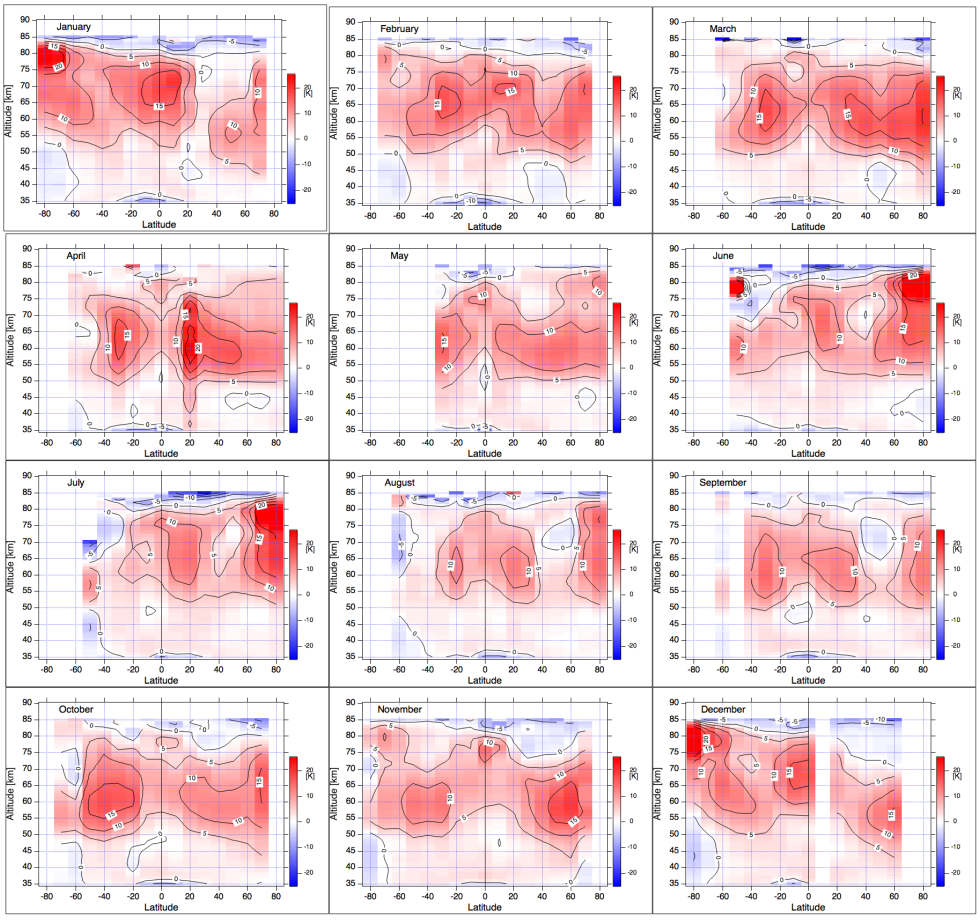

Figure 7. Monthly climatology of the temperature difference between GOMOS and the external (ECMWF+MSIS). Data are averaged over 10° latitude bins.

Atmos. Meas. Tech. Discuss., https://doi.org/10.5194/amt-2018-241
Manuscript under review for journal Atmos. Meas. Tech.
Discussion started: 6 August 2018

Atmospheric Measurement Techniques Discussions

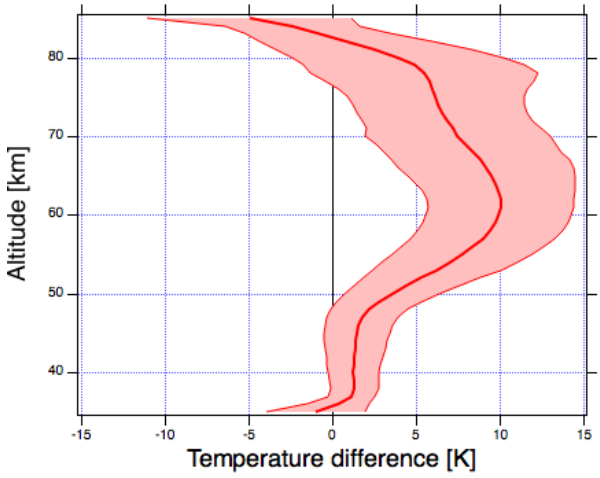

Figure 8. Mean difference between GOMOS Rayleigh temperature and external model temperature as a function of altitude. The standard deviation of the difference is shaded.

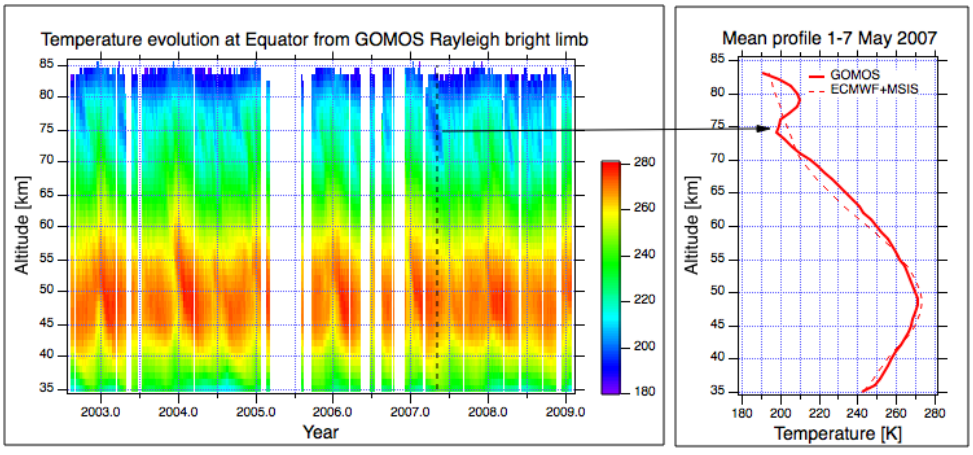

Figure 9. Left) Evolution of the weekly averaged temperature profile at Equator obtained using all occultations of the polar star with a tangent point latitude always situated in the interval 0.8°S-0.8°N. Right) Vertical weekly mean profile beginning of May compared to the GOMOS external model.

Atmos. Meas. Tech. Discuss., https://doi.org/10.5194/amt-2018-241
Manuscript under review for journal Atmos. Meas. Tech.
Discussion started: 6 August 2018

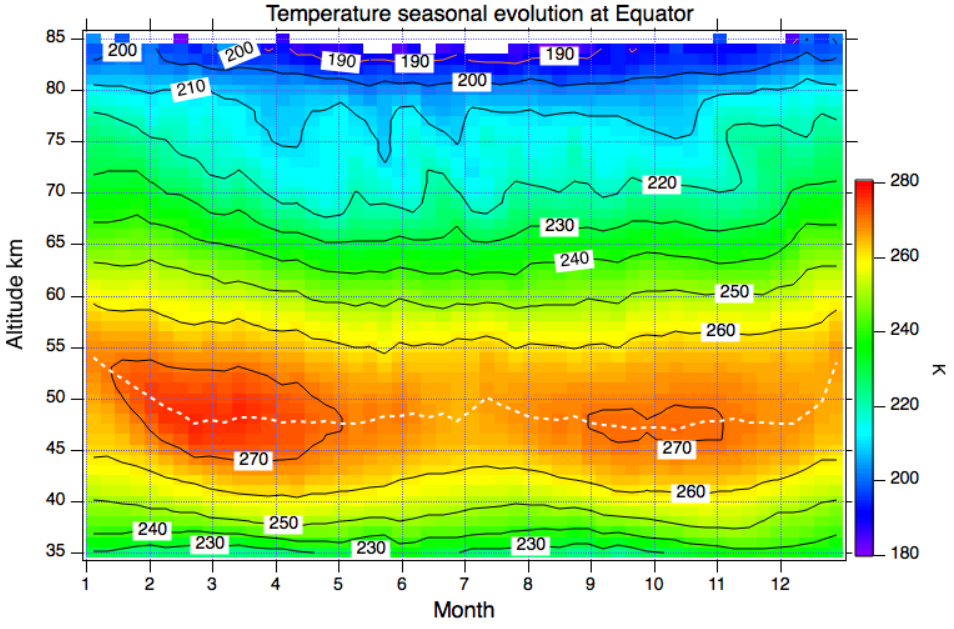

Figure 10. Seasonal evolution of the equatorial temperature derived from temperature data presented in Figure 2. The altitude of the stratopause is indicated by the white dotted line.